

# Singularity structure of the $\pi N$ scattering amplitude in a meson-exchange model up to energies $W \leq 2.0$ GeV

L. Tiator<sup>a</sup>, S.S. Kamalov<sup>a,b,d</sup>, S. Ceci<sup>c</sup>, G.Y. Chen<sup>d</sup>, D. Drechsel<sup>a</sup>, A. Svarc<sup>c</sup>, and S.N. Yang<sup>d</sup>

<sup>a</sup>Institut für Kernphysik, Universität Mainz, D-55099 Mainz, Germany

<sup>b</sup>Bogoliubov Laboratory for Theoretical Physics, JINR, Dubna, 141980 Moscow Region, Russia

<sup>c</sup>Rudjer Boskovic Institute, Division of Experimental Physics, HR-10002 Zagreb, Croatia

<sup>d</sup>Department of Physics and Center for Theoretical Sciences, National Taiwan University, Taipei 10617, Taiwan

(Dated: October 2, 2018)

Within the previously developed Dubna-Mainz-Taipei meson-exchange model, the singularity structure of the  $\pi N$  scattering amplitudes has been investigated. For all partial waves up to  $F$  waves and c.m. energies up to  $W \sim 2$  GeV, the  $T$ -matrix poles have been calculated by three different techniques: analytic continuation into the complex energy plane, speed-plot and the regularization method. For all 4-star resonances, we find a perfect agreement between the analytic continuation and the regularization method. We also find resonance poles for resonances that are not so well established, but in these cases the pole positions and residues obtained by analytic continuation can substantially differ from the results predicted by the speed-plot and regularization methods.

PACS numbers: 11.80.Gw, 13.75.Gx, 14.20.Gk, 25.80.Dj

Keywords: pion-nucleon interaction, baryon resonances, T-matrix poles, speed plot, regularization method

## I. INTRODUCTION

Ever since the  $\Delta(1232)$  resonance was discovered by Fermi and collaborators in 1952 [1–3], the excitation spectrum of the nucleon has played a fundamental role in our understanding of low-energy hadronic physics. The most direct evidence for resonance structure is based on pion-nucleon elastic and charge-exchange scattering. Because total angular momentum, parity, and isospin are conserved within the realm of the strong interaction, the  $S$  matrix for the reactions  $\pi + N \rightarrow \pi' + N'$  may be decomposed into the partial wave amplitudes  $T_{\ell\pm}^I$ , with  $I$  the isospin,  $\ell$  the orbital angular momentum, and the  $\pm$  indicating the total spin of the hadronic system,  $J = \ell \pm \frac{1}{2}$ . Two decades after the discovery of the  $\Delta(1232)$ , a dedicated program at the meson factories had provided enough data to establish a rich resonance spectrum of the nucleon [4, 5]. The further partial wave analysis was driven by studies of the Karlsruhe-Helsinki (KH) [6, 7] and Carnegie-Mellon-Berkeley (CMB) [8, 9] collaborations. In the following years, R. Arndt and coworkers at VPI compiled the data base SAID [10], which was later updated and extended in collaboration with GWU [11, 12]. The works of the CMB, KH, and GW/VPI groups are the main sources of the nucleon resonance listings in the Review of Particle Physics (PDG) [13].

In the most intuitive way, a resonance is an intermediate state of target and projectile that lives longer than in a typical scattering process. Translated into the language of scattering theory, resonances are defined as poles of the  $S$  matrix on unphysical Riemann sheets. Different methods were developed to derive the resonance properties from the observables. In the 1930's it was suggested that a Breit-Wigner function should be a good representation for a resonance pole, and the Breit-Wigner formula for spin zero particles and its generalization to finite spin were developed (see an illustrative discussion in Cottingham and Greenwood, p.241 in Ref. [14]). Later the discussion centered on the rapid increase of the eigenphase shifts through  $90^\circ$  and on the related backward looping of Argand diagrams [15].

However, Breit-Wigner parametrizations have been found to be very model dependent. As was recently shown in the

framework of effective quantum field theory, Breit-Wigner masses are in general field-redefinition dependent [16]. The same model dependency also applies to electromagnetic properties as charges, magnetic moments, transition moments, and form factors. On the other side, all these resonance properties are uniquely defined at the pole of the  $S$  matrix [17].

The analytic properties of the  $S$  matrix are imposed by the principles of unitarity and causality. Because of unitarity, each physical channel leads to a square-root branch point of the partial wave amplitude  $T(W)$  at the respective threshold, with the result that  $T(W)$  is a multi-valued function in the complex  $W$  plane. In particular, a partial wave for elastic  $\pi N$  scattering is described by the amplitudes  $T^{[1]}$  on the physical and  $T^{[2]}$  on the unphysical sheet. The experimental amplitudes are identified with the amplitudes above the cut,  $T_{\text{exp}}(W) = \lim_{\epsilon \rightarrow 0} T^{[1]}(W + i\epsilon)$ , with  $W > M + m$  and  $\epsilon > 0$ . As a consequence, the physical sheet has a discontinuity over the real axis, along the right-hand cut  $M + m \leq W < \infty$ , with  $M$  the nucleon and  $m$  the pion mass. In addition, a relativistic theory has a left-hand cut starting at  $M - m$ . Causality requires that the physical sheet be free of any further singularity, the nucleon resonances should appear as simple poles on the unphysical sheet closest to the real axis of the physical sheet, in agreement with Höhler's remark [18]: *“It is ‘noncontroversial among theorists’ (see Chew [19] and the references in my ‘pole-emics’, p.697 in Ref. [20]) that in  $S$ -matrix theory the effects of resonances follow from first order poles in the 2nd sheet.”* A pole on the second sheet, described by  $T^{[2]}(W) \approx r_p / (M_p - W - i\Gamma_p/2)$ , will often lead to a maximum of the experimental cross section near  $W = M_p$ . The resonance is therefore defined by (i) its pole position in the complex c.m. energy plane at  $W_p = M_p - i\Gamma_p/2$ , with  $M_p$  the real part of the pole position and  $\Gamma_p$  the width of the resonance, and (ii) the residue of the amplitude,  $r_p = |r_p| \exp(i\theta_p)$ , at the pole.

The focus of the present work is on how to extract resonance properties from the data, that is, how do we find a pole in the complex energy plane having at our disposal only data on the real axis and use different pole-extraction methods to extract one, and only one pole per resonance. The problem is how to eliminate the background from the experimental amplitude and to isolate the pole contribution. The time delay method and the related speed plot technique turned out to be the most quantitative tools to detect poles and extract their parameters from the data. A resonance is characterized by a maximum time delay, the time passing between the arrival of a wave packet and its departure from the collision region. In general, a large time delay indicates the formation of an unstable particle in the intermediate state. However, misleading effects can occur by rapid variation of backgrounds, such as narrow cusp effects above  $S$ -wave thresholds or spurious singularities due to phenomenological parametrization of form factors and cut-offs. If a resonance lives long enough, it should decay into all energetically possible final states, unless prevented by general selection rules. Furthermore, the pole position derived from the data should not depend on how the resonance is excited or decays. Whereas such resonances exist in atomic and also in nuclear physics, some caveat is in order for nucleon resonances. As an example, a simple classical model of the  $\Delta(1232)$  leads to the conclusion that the pion stays in its orbit around the nucleon for only about  $100^\circ$  of a full circle.

The pole positions of nucleon resonances have been traditionally derived from the data by the speed plot [4, 21], which is related to the time delay. The “speed” is defined by the slope of the amplitude with energy,  $dT(W)/dW$ , which eliminates constant backgrounds. The speed plot shows the modulus of the speed,  $\text{SP}(W) = |dT(W)/dW|$ , and resonances are identified with peaks in the plot. The resonance parameters are then obtained by fitting the speed of a single pole to the data at physical values of the energy. The idea of the speed plot has been recently generalized to higher derivatives by the “regularization method” (RM) [22]. Within a convergence circle given by the closest neighboring singularity, the Laurent expansion about a pole is given by the sum of  $T^{\text{pole}}(W)$  and a Taylor series

$T^{\text{reg}}(W)$ . With an increasing number of differentiations, the signature of the pole sticks out more and more sharply, whereas more and more leading terms of the Taylor series disappear. It goes without saying that the differentiation of the data will fail after a few steps because of numerical instabilities. However, the regularization method is an interesting tool to study the singularity structure of analytic models. In particular, this method will reveal any rapid variation due to cusp effects and spurious singularities introduced by phenomenological parameterizations.

The inherent model dependence of all the methods has been often overlooked. Examples are the decomposition of the scattering amplitude in a Breit-Wigner form and a background [20] and the fact that eigenphases of a multi-channel system usually do not run through  $90^\circ$  because of the Neumann-Wigner no-crossing theorem [23]. With regard to the latter point, Dalitz and Moorhouse [15] stated: “*With such a complexity of branch cuts without physical significance, we must conclude that the eigenphase representation for the  $S$  matrix is not generally a useful representation for the scattering in the neighborhood of a resonance*”. On the other hand, a single-channel procedure can not reveal much information about resonances ‘far away’ from that channel, that is, if the particular resonance has only a small branching ratio for the particular channel.

The dual nature of the nucleon resonances, the “bare” resonance based on quark configurations and the “dressed” pion-nucleon continuum state, has been studied by several collaborations within Lagrangian models, in particular by EBAC at Jefferson Lab [24, 25], the groups at Giessen [26], Jülich [27], Valencia [28], and Darmstadt [29] as well as the Dubna-Mainz-Taipei collaboration [30]. Such approaches are also the basis for structure investigations of resonances by photo- and electroproduction.

Although Lattice QCD (LQCD) has obtained promising results for the masses and several resonances of the low-lying hadrons [31–33], the large pion mass used and the quenching approximation make it (yet) impossible to treat the resonances as a pion-nucleon scattering state. As shown by Ref. [34] for the  $N\Delta$  form factors, the chiral extrapolation from the stable  $\Delta$  at large pion masses to the experimental pion mass yields unexpected and rather dramatic non-analytic effects at the  $\Delta \rightarrow N\pi$  threshold. The very fact that lattice theory can not yet describe the pion-nucleon final state interaction, makes it impossible to compare the lattice data to the experimental scattering amplitudes in a direct way. However, the LQCD data could be compared to the results of a dynamical model obtained with the same pion mass as used in LQCD. As long as the pion mass is large,  $m_\pi > m_{N^*} - m_N$ , the  $N^*$  appears as an excited bound state. In this case the mass predicted by LQCD should be compared to the “dressed” mass of the dynamical model, which contains the “bare” mass and a real self-energy due to meson loops. In the mass region where the  $N^*$  decays, the LQCD calculation would provide a complex amplitude, comparable to the scattering phases of a partial wave expansion. Based on the work of Lüscher [35], the width of the rho meson [36] and of the Delta resonance [37] have been recently studied. In such a case the lattice data can be treated like experimental amplitudes, that is, by speed plot or Breit-Wigner analyses. However, as long as the LQCD pion mass lies above the physical value, an extrapolation to the physical pion mass will still be necessary by use of a dynamical model or an effective field theory.

In the present contribution we study the Dubna-Mainz-Taipei model (DMT) [30] by comparing the pole parameters resulting from analytic continuation with approximate procedures such as the speed plot and the regularization method. The DMT model is a field-theoretical meson-exchange model for  $\pi N$  scattering. In contrast to the partial wave amplitudes obtained in Refs. [8–12], which inevitably involve a smoothing of the data, the energy dependence of the DMT amplitudes is largely determined from theoretical considerations even though there are free parameters in

the model. Another strong point of the DMT model is the fact that the prescribed background contribution, a major source of the model dependence for the resonance extraction procedure, has been found to give excellent agreement if applied to low energy electromagnetic pion production [38]. In Sect. II we give an overview of the speed-plot, time-delay, and regularization methods to derive the pole parameters. The Dubna-Mainz-Taipei model is presented in Sect. III, in particular with regard to the definitions of resonant vs. background terms as well as form factors and cut-offs. Our results for the resonance parameters are reported in Sect. IV, and the different techniques to derive these parameters are compared. We conclude with a summary and outlook in Sect. V.

## II. HOW TO FIND A RESONANCE

### A. Time delay

In the framework of a potential scattering problem, resonance phenomena are related to the formation and the decay of intermediate quasi-stationary states. An ideal resonance should decay in all energetically possible final states, unless forbidden by selection rules for a specific channel. Provided that the interaction is of short range, resonances can be characterized by the *time delay* between the arrival of a wave packet and its departure from the collision region. In general, the time delay shows a pronounced peak at the resonance energies. The time delay was introduced by Eisenbud in his Ph.D. thesis [39] and later applied to multi-channel scattering theory by Smith [40]. Following the work of Refs. [15, 41–43], we define the time delay for a single-channel scattering problem in a partial wave as follows:

$$\Delta t(W) = \text{Re} \left( -i \frac{1}{S(W)} \frac{dS(W)}{dW} \right) = 2 \frac{d\delta(W)}{dW}, \quad (1)$$

where  $S(W) = \exp[2i\delta(W)]$  is the  $S$  matrix and  $\delta(W)$  the scattering phase shift. A simple ansatz for a unitary  $S$  matrix with a pole at  $W_p = M_p - \frac{i}{2}\Gamma_p$  and a constant background phase  $\delta_B$  is given by

$$S(W) = \frac{M_p + \frac{i}{2}\Gamma_p - W}{M_p - \frac{i}{2}\Gamma_p - W} e^{2i\delta_B} = e^{2i\delta_R(W)} e^{2i\delta_B}, \quad (2)$$

where  $\delta_R(W) = \arctan[\frac{1}{2}\Gamma_p/(M_p - W)]$  is the resonant phase. The related  $T$ -matrix  $T = (S - 1)/(2i)$  and the real matrix  $K = i(1 - S)(1 + S)^{-1}$  take the forms

$$T(W) = \frac{\frac{1}{2}\Gamma_p}{M_p - \frac{i}{2}\Gamma_p - W} e^{2i\delta_B} + \sin\delta_B e^{i\delta_B}, \quad (3)$$

$$K(W) = \frac{\frac{1}{2}\Gamma_p + (M_p - W)\tan\delta_B}{M_p - W - \frac{1}{2}\Gamma_p\tan\delta_B}. \quad (4)$$

Combining Eqs. (1) and (2), we obtain a simple Breit-Wigner form for the time delay,

$$\Delta t(W) = \frac{\Gamma_p}{(W - M_p)^2 + \frac{1}{4}\Gamma_p^2}. \quad (5)$$

In this ideal case, the maximum time delay is  $\Delta t(M_p) = 4/\Gamma_p$ . We observe that both the real ( $M_p$ ) and imaginary ( $-\frac{1}{2}\Gamma_p$ ) parts of the pole position are determined by the time delay (and therefore also by the scattering matrix) at real (physical!) values of the c.m. energy  $W$ .

In order to describe a system of coupled channels, the lifetime matrix  $Q$  was introduced [40],

$$Q_{ij}(W) = -i \frac{dS_{ik}(W)}{dW} S_{jk}^*(W). \quad (6)$$

The analog of the time delay for a multi-channel system was found to be the trace of  $Q$  as function of  $W$ . This trace takes a more transparent form after diagonalization of the  $S$  matrix [15, 44],

$$\text{tr}[Q(W)] = 2 \sum_{\alpha} \frac{d\delta_{\alpha}(W)}{dW}, \quad (7)$$

with  $\delta_{\alpha}$  the eigenphase shifts. However, a realistic application of the lifetime matrix requires the knowledge of all open channels, that is, the reactions  $\pi N \rightarrow \pi N$ ,  $\pi N \rightarrow \pi\pi N$ ,  $\pi\pi N \rightarrow \pi\pi N$ ,  $\pi N \rightarrow \eta N$ , and so on. As a consequence of Wigner's no-crossing theorem [45], individual eigenphases have a complicated energy dependence. It is therefore only the sum of the eigenphases that shows distinct resonance structures. Based on this observation, it has been recently proposed to search for resonance parameters by studying the traces of multi-channel  $T$  and  $K$  matrices [46, 47]. The respective scattering matrices were constructed from experimental data for the  $\pi N$  and  $\eta N$  channels and models for the two-pion channels.

### B. Speed plot

The *speed plot* of a partial wave amplitude  $T$  is defined by

$$\text{SP}(W) = \left| \frac{dT(W)}{dW} \right|. \quad (8)$$

As was recognized by the Particle Data Group already in the early 1970's, the speed plot is a convenient tool to extract the pole position of a resonance [5, 48]. This technique was intensively studied by Höhler who wanted to extract resonance parameters from the Karlsruhe-Helsinki partial wave analysis (KH80) [21, 49]. Because the KH analysis was restricted to elastic pion-nucleon scattering, a multi-channel treatment like the construction of the lifetime matrix was out of reach.

For a single channel system, the time delay and the speed plot are identical up to a factor 2. In particular, the ansatz of Eq. (3) leads to the speed

$$\text{SP}(W) = \frac{\frac{1}{2}\Gamma_p}{(W - M_p)^2 + \frac{1}{4}\Gamma_p^2}. \quad (9)$$

As a result, the speed plot shows a maximum for  $W = M_p$ , which defines the real part of the pole position in the complex  $W$  plane. The imaginary part of the pole position can be obtained from the relation

$$\text{SP}(M_p \pm \frac{1}{2}\Gamma_p) = \frac{1}{2} \text{SP}(M_p). \quad (10)$$

In practical applications, this straightforward method is numerically not very stable and fails completely for the  $S_{11}(1535)$  resonance, which is very close to the  $\eta$  threshold. In order to allow for inelasticities, we therefore assume the functional form

$$T(W) = \frac{r_p}{M_p - W - \frac{i}{2}\Gamma_p} \quad (11)$$

with  $r_p$ , the complex residue at the pole, given by

$$\text{Res } T(W)|_{W=W_p} = - |r_p| e^{i\theta_p}. \quad (12)$$

For a single (elastic) channel, the comparison with Eq. (3) yields the residue. The more general ansatz Eq. (11) leads to the speed

$$\text{SP}(W) = \frac{|r_p|}{(W - M_p)^2 + \frac{1}{4}\Gamma_p^2}, \quad (13)$$

which is fitted to speed data obtained from the partial wave amplitudes in the vicinity of the maximum. The pole parameters  $M_p, \Gamma_p$  and  $|r_p|$  are then obtained from the best fit to the selected speed points. Finally, the phase  $\theta_p$  of the residue is obtained from the phase of  $dT/dW$ ,

$$\tan \theta_p = \frac{\text{Im}(dT/dW)}{\text{Re}(dT/dW)} \Big|_{W=M_p}. \quad (14)$$

### C. Regularization method

As discussed before, the speed plot technique is successful if the background under the resonance is approximately constant. It fails if the background changes over the resonance region. The *regularization method* extends the idea behind the speed plot by construction of higher derivatives,  $T^{(N)} \equiv d^N T/dW^N$ ,  $N \geq 1$  [22]. Let there be an analytic function  $T(z)$  of a complex variable  $z$  with a first-order pole at some complex point  $\mu = x + iy$ . This function can be any of the  $T$ -matrix elements, and the variable  $z$  is identified with the c.m. energy  $W$  in order to compare with the speed plot technique. The described function takes the form

$$T(z) = \underbrace{\frac{r}{\mu - z}}_{\text{resonant part}} + \underbrace{\left(T(z) - \frac{r}{\mu - z}\right)}_{\text{smooth background}}, \quad (15)$$

where  $\mu$  and  $r$  are the position and residue of the pole. Of course, the experiment can determine the  $T$ -matrix elements only for real values of  $W$ . In order to continue  $T(W)$  into the complex energy plane and to search for the pole position, we construct a regular function  $f$  by multiplying  $T$  with the factor  $\mu - z$ ,

$$f(z) = (\mu - z)T(z), \quad (16)$$

with  $f(\mu) = r$ . In the neighborhood of the pole, the function  $f$  can be expanded in a Taylor series. Because the scattering matrix can be accessed for real arguments only, we construct  $f(\mu)$  from the derivatives of  $f$  taken along the real axis,

$$r = f(\mu) = \sum_{n=0}^N \frac{f^{(n)}(W)}{n!} (\mu - W)^n + R_N(W, \mu). \quad (17)$$

This expansion is explicitly written to order  $N$ , and  $R_N(W, \mu)$  stands for the higher orders. The derivatives  $f^{(n)}(W)$  can be turned in derivatives of the  $T$  matrix by use of Eq. (16), and mathematical induction leads to the following equation:

$$f^{(n)}(W) = (\mu - W)T^{(n)}(W) - nT^{(n-1)}(W). \quad (18)$$

Insertion of these derivatives into Eq. (16) cancels all the terms in the sum except for the last one,

$$r = \frac{T^{(N)}(W)}{N!} (\mu - W)^{(N+1)} + R_N(W, \mu). \quad (19)$$

In the neighborhood of the pole, the remainder  $R_N$  should decrease with increasing  $N$ . Assuming that the higher derivatives can be neglected for a sufficiently large value of  $N$  and taking the absolute values of both sides, we obtain an approximation of the pole parameters at  $\mathcal{O}(N)$ ,

$$|r_N| = \frac{|T^{(N)}(W)|}{N!} |\mu_N - W|^{(N+1)}. \quad (20)$$

On condition that the Taylor series converges and in the limit  $N \rightarrow \infty$ ,  $r_N$  and  $\mu_N$  should approach the values  $r$  and  $\mu$ , respectively. In the next step, we (i) write the pole position as a general complex number,  $\mu = a + ib$ , (ii) raise both sides of Eq. (20) to the power of  $2/(N+1)$ , and collect the information about the  $T$ -matrix and the pole position on the right and left side, respectively. The result is a parabolic equation in  $W$ ,

$$\frac{(a_N - W)^2 + b_N^2}{\sqrt[N+1]{|r_N|^2}} = \sqrt[N+1]{\frac{(N!)^2}{|T^{(N)}(W)|^2}}. \quad (21)$$

This equation relates the pole position ( $a = M_p$ ,  $b = -\frac{i}{2} \Gamma_p$ ) and the absolute value of the residue,  $|r|$ , to the  $T$ -matrix values on the real axis, as obtained from a model or an energy-dependent partial-wave analysis of the data. Finally, the phase of the residue is determined by

$$\tan \theta_N = \frac{\text{Im } T^{(N)}(W)}{\text{Re } T^{(N)}(W)} \Big|_{W=M_p}. \quad (22)$$

The comparison of the above equations with the results of Sect. II B shows that the speed plot is identical to the regularization method for  $N = 1$ .

The further procedure is as follows: (i) Construct the  $N^{\text{th}}$  derivative of the  $T$ -matrix element and the right-hand side of Eq. (21). Note that the pole parameters are uniquely determined by the *exact* knowledge of  $T(W)$  in only *three points*. However, the problem is to choose the right points. If the distance between the points gets too large, the influence of other singularities may increase. If the points are too close, numerical problems may occur. (ii) Solve Eq. (21) for the pole parameters by either choosing various three-point sets to evaluate the right-hand side and perform a statistic analysis of the results or fitting the right-hand side of the equation to a three-parameter parabolic function. In our approach we have chosen the latter option.

In closing this section we note that the regularization method does not depend on any particular functional form of the  $T$  matrix. However, we have to assume that (a) the  $N^{\text{th}}$  derivative can be constructed with a sufficient precision and (b) the pole position lies within the circle of convergence for the Taylor expansion, that is, no further singularities should intrude into the region between the pole and the related resonance region on the real  $W$  axis.

#### D. Poles from analytic continuation

The most accurate way to determine pole positions and residues is certainly obtained by analytic continuation into the complex region. Because resonance poles can not appear on the physical sheet, we have to take a careful look at the structure of different Riemann sheets opening at all branch points for particle production in a coupled-channels model. The most important particle thresholds in our energy region below 2 GeV are  $\pi\pi N$ ,  $\pi\Delta$ ,  $\eta N$ , and  $\rho N$  with branch points at 1178 MeV,  $(1350 - 50i)$  MeV, 1486 MeV, and  $(1713 - 75i)$  MeV, in order. In the dynamical DMT model we have included the  $\pi N$  and  $\pi\pi N$  channels in all the partial waves and the  $\eta N$  channel in the  $S_{11}$  partial

wave. However, the  $\pi\pi N$  channel is treated in a phenomenological way as will be described in the following section. Because the particular ansatz for the two-pion width, Eq. (43), contains only even powers of  $q_{2\pi}$ , the model does not give additional branch points for the two-pion channel. This leads to a relatively simple sheet structure, and we can easily reach the poles on the most important second Riemann sheet (first unphysical sheet). Technically, we first map the relevant region on this sheet by contour plots and search for the accurate pole position by standard root finding routines applied to the function

$$h(z_p) = \frac{1}{|T(z_p)|} = 0. \quad (23)$$

Next we obtain the residue by approaching the pole along different paths in the complex plane,

$$\text{Res } T(z)|_{z_p} = \lim_{z \rightarrow z_p} (z - z_p) T(z). \quad (24)$$

A word of caution is in order. If the fitted form factor parameters, e.g.,  $\Lambda_\alpha$  of Eq. (37) or  $X_R$  of Eq. (43) become smaller than about 500 MeV, additional poles can appear in the region where the resonance poles are expected. In order to avoid such spurious singularities, it is very important to map out the structure of the  $T$  matrix very precisely. Also the speed-plot and regularization methods are very helpful to distinguish between resonance and spurious poles, because the latter ones usually affect  $T$  matrix at real  $W$  in a similar way as a broad background does.

### III. THE DUBNA-MAINZ-TAIPEI MESON-EXCHANGE MODEL

The Dubna-Mainz-Taipei (DMT)  $\pi N$  meson-exchange model was developed on the basis of the Taipei-Argonne  $\pi N$  meson-exchange model [50–52] which describes pion-nucleon scattering up to 400 MeV pion laboratory energy. The DMT model was extended to c.m. energies  $W = 2.0$  GeV by inclusion of higher resonances and the  $\eta N$  channel [30, 53]. The model gives an excellent fit to both  $\pi N$  phase shifts and inelasticity parameters in all the channels up to the  $F$  waves and energies of 2 GeV, except for the  $F_{17}$  partial wave. The DMT  $\pi N$  model is also a main ingredient of the Dubna-Mainz-Taipei dynamical model describing the photo- and electroproduction of pions [54] up to 2 GeV. In particular, this model gives an excellent agreement with pion production data from threshold to the first resonance region [38, 55]. In this section, we briefly outline the ingredients of the Taipei-Argonne  $\pi N$  model and then describe some relevant features of the DMT meson-exchange coupled-channels model.

#### A. Taipei-Argonne meson-exchange $\pi N$ model

The Taipei-Argonne model describes the elastic scattering of pions and nucleons. It is based on a three-dimensional reduction of the Bethe-Salpeter equation for an effective Lagrangian involving  $\pi$ ,  $N$ ,  $\Delta$ ,  $\rho$ , and  $\sigma$  fields. Let us first describe some kinematics for  $\pi N$  scattering,

$$\pi(q) + N(p) \rightarrow \pi(q') + N(p'), \quad (25)$$

where  $q, p, q'$ , and  $p'$  are the four-momenta of the respective particles. The total and relative four-momenta are  $P = p + q$  and  $k = p \eta_\pi(s) - q \eta_N(s)$ , respectively, where  $s = P^2 = W^2$  is the Mandelstam variable. The dimensionless variables  $\eta_\pi(s)$  and  $\eta_N(s)$  represent the freedom in choosing a three-dimensional reduction, they are constrained by the condition  $\eta_N + \eta_\pi = 1$ . For further details we refer to Ref. [52].



The Bethe-Salpeter equation for  $\pi N$  scattering takes the form

$$T_{\pi N} = B_{\pi N} + B_{\pi N} G_0 T_{\pi N}, \quad (26)$$

where  $B_{\pi N}$  is the sum of all irreducible two-particle Feynman amplitudes and  $G_0$  the free relativistic pion-nucleon propagator. Equation (26) can be cast into the form

$$T_{\pi N} = \hat{B}_{\pi N} + \hat{B}_{\pi N} \hat{G}_0 T_{\pi N}, \quad (27)$$

with

$$\hat{B}_{\pi N} = B_{\pi N} + B_{\pi N} (G_0 - \hat{G}_0) \hat{B}_{\pi N}, \quad (28)$$

where  $\hat{G}_0(k; P)$  is an appropriate propagator to obtain a three-dimensional reduction of Eq. (26). This propagator is chosen to maintain the two-body unitarity by reproducing the  $\pi N$  elastic cut. However, there is still a wide range of possible propagators satisfying this constraint. A standard choice is the Cooper-Jennings reduction scheme [56],

$$\begin{aligned} \hat{G}_0(k; P) &= \frac{1}{(2\pi)^3} \int \frac{ds'}{s-s'} f(s, s') [\alpha(s, s') \not{P} + \not{k} + m_N] \\ &\quad \times \delta^{(+)}([\eta_N(s')P' + k]^2 - m_N^2) \delta^{(+)}([\eta_\pi(s')P' - k]^2 - m_\pi^2), \end{aligned} \quad (29)$$

with  $P' = \sqrt{s'/s} P$  and the superscript (+) of the  $\delta$ -functions standing for the positive energy part of the propagator. The variables  $f$  and  $\alpha$  are dimensionless variables containing the freedom of reduction, they are constrained by the conditions  $f(s, s) = 1$  and  $\alpha(s, s) = \eta_N(s)$  to ensure the reproduction of the elastic cut. Furthermore, Cooper and Jennings define [56]

$$\alpha(s, s') = \eta_N(s), \quad f(s, s') = \frac{4\sqrt{ss'}\varepsilon_N(s')\varepsilon_\pi(s')}{ss' - (m_N^2 - m_\pi^2)^2}, \quad (30)$$

which leads to the following expression for  $\hat{G}_0$  in the c.m. frame:

$$\hat{G}_0(k; s) = \frac{1}{(2\pi)^3} \frac{\delta[k_0 - \hat{\eta}(s_{\vec{k}}, \vec{k})]}{\sqrt{s} - \sqrt{s_{\vec{k}}}} \frac{2\sqrt{s_{\vec{k}}}}{\sqrt{s} + \sqrt{s_{\vec{k}}}} f(s, s_{\vec{k}}) \frac{\alpha(s, s_{\vec{k}}) \gamma_0 \sqrt{s} + \not{k} + m_N}{4E_N(\vec{k})E_\pi(\vec{k})}, \quad (31)$$

where  $E_N(\vec{k})$  and  $E_\pi(\vec{k})$  are the nucleon and pion energies for the three-momentum  $\vec{k}$ ,  $\sqrt{s_{\vec{k}}} = E_N(\vec{k}) + E_\pi(\vec{k})$  is the total energy in the c.m. frame, and  $\hat{\eta}(s, \vec{k}) = E_N(\vec{k}) - \eta_N(s_{\vec{k}})\sqrt{s_{\vec{k}}}$ . With these relations we obtain the following  $\pi N$  scattering equation:

$$t(\vec{k}', \vec{k}; W) = v(\vec{k}', \vec{k}; W) + \int dk'' v(\vec{k}', \vec{k}''; W) g_0(\vec{k}''; W) t(\vec{k}'', \vec{k}; W). \quad (32)$$

The explicit relations between the quantities defined by Eqs. (26) and (32) are given by

$$t(\vec{k}', \vec{k}; W) = \int dk'_0 dk_0 \delta(k'_0 - \hat{\eta}') T(k', k; W) \delta(k_0 - \hat{\eta}), \quad (33)$$

$$v(\vec{k}', \vec{k}; W) = \int dk'_0 dk_0 \delta(k'_0 - \hat{\eta}') B(k', k; W) \delta(k_0 - \hat{\eta}), \quad (34)$$

$$g_0(\vec{k}; W) = \int dk_0 \hat{G}_0(k; W), \quad (35)$$

with  $\hat{\eta}' = \hat{\eta}(s_{\vec{k}'}, \vec{k}')$  and  $\hat{\eta} = \hat{\eta}(s_{\vec{k}}, \vec{k})$ .

The effective Lagrangian involving the  $\pi, N, \sigma, \rho,$  and  $\Delta(1232)$  fields takes the form

$$\begin{aligned}
\mathcal{L}_I = & \frac{f_{\pi NN}^{(0)}}{m_\pi} \bar{N} \gamma_5 \gamma_\mu \vec{\tau} \cdot \partial^\mu \vec{\pi} N - g_{\sigma\pi\pi}^{(s)} m_\pi \sigma (\vec{\pi} \cdot \vec{\pi}) - \frac{g_{\sigma\pi\pi}^{(v)}}{2m_\pi} \sigma (\partial^\mu \vec{\pi} \cdot \partial_\mu \vec{\pi}) - g_{\sigma NN} \bar{N} \sigma N \\
& - g_{\rho NN} \bar{N} \{ \gamma_\mu \vec{\rho}^\mu + \frac{\kappa_V^\rho}{4m_N} \sigma_{\mu\nu} (\partial^\mu \vec{\rho}^\nu - \partial^\nu \vec{\rho}^\mu) \} \cdot \frac{1}{2} \vec{\tau} N \\
& - g_{\rho\pi\pi} \vec{\rho}^\mu \cdot (\vec{\pi} \times \partial_\mu \vec{\pi}) - \frac{g_{\rho\pi\pi}}{4m_\rho^2} (\delta - 1) (\partial^\mu \vec{\rho}^\nu - \partial^\nu \vec{\rho}^\mu) \cdot (\partial_\mu \vec{\pi} \times \partial_\nu \vec{\pi}) \\
& + \frac{g_{\pi N \Delta}}{m_\pi} \bar{\Delta}_\mu [g^{\mu\nu} - (Z + \frac{1}{2}) \gamma^\mu \gamma^\nu] \vec{T}_{\Delta N} N \cdot \partial_\nu \vec{\pi}, \tag{36}
\end{aligned}$$

with  $\Delta_\mu$  the Rarita-Schwinger field operator for the  $\Delta$  resonance and  $\vec{T}_{\Delta N}$  the isospin transition operator between nucleon and  $\Delta$ . The driving term  $B_{\pi N}$  in Eq. (26) is approximated by the tree diagrams of the interaction Lagrangian of Eq. (36), the direct and crossed  $N$  and  $\Delta$  diagrams as well as the t-channel  $\sigma$ - and  $\rho$ -exchange contributions.

Furthermore, the driving term  $v(\vec{k}, \vec{k}'; W)$  of Eq. (34) is regularized by covariant form factors associated with each leg of the vertices,

$$F_\alpha(p_\alpha^2) = \left[ \frac{n\Lambda_\alpha^4}{n\Lambda_\alpha^4 + (m_\alpha^2 - p_\alpha^2)^2} \right]^n, \tag{37}$$

with  $p_\alpha$  the four-momentum and  $m_\alpha$  the mass of particle  $\alpha$ . In the present work we choose the value  $n = 10$  as used by Ref. [53].

As in the work of Afnan and collaborators [57, 58], the  $P_{11}$  phase shift is constrained by imposing the nucleon pole condition. This treatment leads to a proper renormalization of both nucleon mass and  $\pi NN$  coupling constant. It also yields the necessary cancelation between the repulsive nucleon pole contribution and the attractive background, such that a reasonable fit to the  $\pi N$  phase shifts in the  $P_{11}$  channel can be achieved.

The following parameters were allowed to vary in the fit procedure: the products  $g_{\sigma NN} g_{\sigma\pi\pi}^{(s)}$ ,  $g_{\sigma NN} g_{\sigma\pi\pi}^{(v)}$ , and  $g_{\rho NN} g_{\rho\pi\pi}$  as well as  $\delta$  for the t-channel  $\sigma$  and  $\rho$  exchanges,  $m_\Delta^{(0)}$ ,  $g_{\pi N \Delta}^{(0)}$ , and  $Z$  for the  $\Delta$  mechanism, and the cut-off parameters  $\Lambda_\alpha$  of the form factors given by Eq. (37). The experimental  $\pi N$  phase shifts were well described up to pion laboratory energies of 400 MeV. The resulting parameters and predicted phase shifts can be found in Ref. [52].

## B. DMT meson-exchange model including $\eta N$ channel and higher resonances

As the energy gets larger, heavier mass channels like  $\sigma N$ ,  $\eta N$ ,  $\pi\Delta$ , and  $\rho N$  as well as a non-resonant continuum of  $\pi\pi N$  states become increasingly important, and at the same time more and more nucleon resonances appear as intermediate states. For each contributing resonance  $R$ , the Hilbert space is enlarged by a bare resonance  $R$  which acquires a width by its coupling to the  $\pi N$  and  $\eta N$  channels through the Lagrangian

$$\mathcal{L}_I = ig_{\pi NR}^{(0)} \bar{R} \tau N \cdot \pi + ig_{\eta NR}^{(0)} \bar{R} N \eta + \text{h.c.}, \tag{38}$$

where  $N, R, \pi,$  and  $\eta$  denote the field operators for the nucleon, bare resonance  $R$ , pion, and eta meson, respectively. The full  $t$ -matrix can be written as a system of coupled equations,

$$t_{ij}(W) = v_{ij}(W) + \sum_k v_{ik}(W) g_k(W) t_{kj}(W), \tag{39}$$

with  $i$  and  $j$  denoting the  $\pi$  and  $\eta$  channels and  $W$  is the total c.m. energy.

In general, the potential  $v_{ij}$  is the sum of non-resonant ( $v_{ij}^B$ ) and bare resonance ( $v_{ij}^R$ ) terms,

$$v_{ij}(W) = v_{ij}^B(W) + v_{ij}^R(W). \quad (40)$$

The non-resonant term  $v_{\pi\pi}^B$  for the  $\pi N$  elastic channel, as defined in Sec. III A, contains contributions from  $s$ - and  $u$ -channel Born terms as well as  $t$ -channel contributions with  $\omega$ ,  $\rho$ , and  $\sigma$  exchange. The parameters in  $v_{\pi\pi}^B$  are fixed by an analysis of the pion scattering phase shifts for the  $S$  and  $P$  waves at energies  $W < 1300$  MeV [52]. In the channels involving the  $\eta$ , the potential  $v_{i\eta}^B$  is assumed to vanish because of the small  $\eta NN$  coupling [59].

The bare resonance contribution arises from the excitation and decay of the resonance  $R$ ,

$$v_{ij}^R(W) = \frac{h_{iR}^{(0)\dagger} h_{jR}^{(0)}}{W - M_R^{(0)}}, \quad (41)$$

where  $M_R^{(0)}$  and  $h_{iR}^{(0)}$  denote the bare mass for the resonance  $R$  and the bare vertex operator  $R \rightarrow \pi/\eta + N$ , respectively. The matrix elements of the potential  $v_{ij}^R(W)$  is symbolically expressed by

$$v_{ij}^R(q, q'; W) = \frac{f_i(\tilde{\Lambda}_i, q; W) g_i^{(0)} g_j^{(0)} f_j(\tilde{\Lambda}_j, q'; W)}{W - M_R^{(0)} + \frac{i}{2} \Gamma_R^{2\pi}(W)}, \quad (42)$$

where  $q$  and  $q'$  are the pion (or eta) momenta in the initial and final states, and  $g_{i/j}^{(0)}$  denotes the resonance vertex couplings. As in Ref. [52], we associate a covariant form factor with each leg of the vertices. Therefore, each vertex  $f_i$  in Eq. (42) contains three form factors as given by Eq. (37), and  $\tilde{\Lambda}_i$  stands for a triple of cut-offs,  $(\Lambda_N, \Lambda_R, \Lambda_\pi)$ . In Eq. (42) we have also included a phenomenological term  $\Gamma_R^{2\pi}(W)$  in the resonance propagator to account for the  $\pi\pi N$  decay channel. Therefore, our ‘‘bare’’ resonance propagator already contains a phenomenological ‘‘dressing’’ effect due to the coupling to the  $\pi\pi N$  channel. With this prescription we assume that any further non-resonant coupling to the  $\pi\pi N$  channel can be neglected. Following Refs. [60, 61] we parameterize the two-pion width by

$$\Gamma_R^{2\pi}(W) = \Gamma_R^{2\pi(0)} \left( \frac{q_{2\pi}}{q_0} \right)^{2\ell+4} \left( \frac{X_R^2 + q_0^2}{X_R^2 + q_{2\pi}^2} \right)^{\ell+2}, \quad (43)$$

where  $\ell$  is the pion orbital momentum and  $q_{2\pi} = q_{2\pi}(W)$  the momentum of the compound two-pion system. Furthermore, the two-pion width and two-pion momentum at resonance are denoted by  $\Gamma_R^{2\pi(0)}$  and  $q_0$ , respectively. We note that this form accounts for the correct energy behavior of the phase space near the three-body threshold [60]. In our present work,  $\Gamma_R^{2\pi(0)}$  and  $X_R$  are considered as free parameters. Therefore, each resonance is generally described by 6 free parameters, the bare mass  $M_R^{(0)}$ , the decay width  $\Gamma_R^{2\pi(0)}$ , two bare coupling constants  $g_i^{(0)}$  and  $g_j^{(0)}$ , and two cut-off parameters  $\Lambda_R$  and  $X_R$ . The generalization of the coupled-channel model to the case of  $N$  resonances with the same quantum numbers is then given by

$$v_{ij}^R(q, q'; W) = \sum_{n=1}^N v_{ij}^{R_n}(q, q'; W), \quad (44)$$

with 6 free parameters for each resonance.

The solutions of the coupled-channel equations of Eq. (39), with potentials given in Eqs. (40-43), were fitted to the experimental  $\pi N$  phase shifts and inelasticities by variation of the bare resonance parameters. The fit gave a good agreement with the data for all channels up to the  $F$  waves and energies below 2 GeV, except for the partial wave  $F_{17}$  [30]. The predictions of the DMT model for the resonance parameters are presented in the next section.

## IV. RESULTS AND DISCUSSION

In this section we present the nucleon resonance parameters as derived from the DMT model. The listed resonances fulfill the following criteria: (i) the pole position is restricted by  $M_p \leq 2$  GeV and  $\Gamma_p \leq 0.4$  GeV, (ii) the residue is larger than about 1 MeV, and (iii) the branching ratio for the one-pion channel is limited by  $2r_p/\Gamma_p \geq 10$  %. Furthermore, the pole position obtained by the renormalization method has to be stable over a range of derivatives (N values).

### A. S-waves

As reported in Ref. [53], we need four  $S_{11}$  resonances to fit the  $\pi N$  scattering amplitude in this channel, instead of the three resonances listed by the PDG [13]. The additional resonance  $S_{11}(1878)$  was found to play an important role in pion photoproduction as well [53], but was not seen in both the  $\pi N \rightarrow \eta N$  reaction and recent measurements of  $\eta$  photoproduction from the proton [62, 63]. However, in the analysis of Durand *et al.* [64, 65] on eta photoproduction a new  $S_{11}$  state of mass  $M = 1707$  MeV and width  $\Gamma = 222$  MeV was needed in order to get good agreement with the data.

In our analysis (see Fig. 1, left panel) we find four poles, three of them below 2 GeV. The exact pole positions are shown by asterisks with a size proportional to their relative strength. Furthermore, the ranges of the PDG pole values are displayed by open boxes. The first resonance  $S_{11}(1535)^{****}$  is well found by both speed-plot and regularization methods. The second state, the  $S_{11}(1650)^{****}$  is even better described, with some improvement by the regularization method. The third state is very weakly excited in the  $\pi N$  interaction and can not be seen by the SP, whereas the RM finds a state close by. A fourth state, slightly above 2 GeV and classified by PDG as 1-star  $S_{11}(2090)^*$  is also found by SP and RM at close-by positions.

For the isospin 3/2 state we obtain three poles in agreement with PDG. The first one,  $S_{31}(1620)^{****}$  is nicely described by SP and perfectly by RM. The second pole,  $S_{31}(1900)^{**}$  is similarly well seen by both SP and RGM. The third resonance,  $S_{31}(2150)^*$ , lies far down in the imaginary region. Only the SP locates a state in the expected energy region, however, with only a small fraction of the residue can be obtained.

### B. P-waves

For the  $P$ -wave resonances we show our results in Fig. 2. In the  $P_{11}$  partial wave we get 3 poles, all of them being somehow related to the 3 PDG states. However, our second and third pole positions lie further down in the negative imaginary region, the third pole is even below the range shown in the figure. The position of the first resonance, the Roper  $P_{11}(1440)^{****}$  is very well described by both SP and RM. The two higher states have very weak signals in the  $\pi N$  amplitude. Although the RM yields a considerable improvement over the SP, it also misses the exact pole position.

From the results in Table II we find that only a very small fraction of the residue can be found with these techniques. This is a general property for poles lying far away from the real axis. A detailed analysis of the contour for this partial wave also shows a zero position sitting closely above the pole position, and therefore masking the pole if searched for along the real axis.

In the  $P_{13}$  partial wave we also find three poles. Two of them are very well reproduced by RM. PDG lists only two states, the  $P_{13}(1720)^{****}$  with a large error bar for the imaginary part and the  $P_{13}(1900)^{**}$ , however, with no pole position data given. Our results for the  $P_{13}(1720)^{****}$  lie close to the PDG values, with the imaginary part close to the lower limit of PDG error bar.

The isospin-3/2 partial wave,  $P_{31}$  is an exceptional case. Here the lowest state is not the dominant one, and also the PDG lists a  $P_{31}(1750)^{**}$  without pole values. We find a lowest pole near 1800 MeV with a very large imaginary value outside of our considered range. The dominant  $P_{31}(1900)^{****}$  lies only slightly outside the PDG box and is very well described by RM.

The Delta resonance,  $P_{33}(1232)^{****}$ , has of course the largest strength of all the poles found in our analysis. It is very well described by both the SP and RM techniques and coincides with PDG. Two further, rather weakly excited  $P_{33}$  states are found at higher energies, which can be related to the states  $P_{33}(1600)^{***}$  and  $P_{33}(1920)^{***}$  reported by PDG. While the analytic result for the  $P_{33}(1600)^{***}$  agrees fairly well with RM, the  $P_{33}(1920)^{***}$  lies outside of the considered range.

### C. D-waves

In Fig. 3 we show the poles of  $D$ -wave resonances. PDG lists three  $J = 3/2$  states with isospin 1/2,  $D_{13}(1520)^{****}$ ,  $D_{13}(1700)^{***}$  and  $D_{13}(2080)^{**}$ , but even a total number of four regions with extracted pole values, three of these PDG boxes show up in our figure. Our analysis agrees very well within the reported ranges, where we also locate four resonance states. While the dominant first resonance is perfectly described by SP and RM, the SP can only locate another (third) pole. The improved RM technique, however, is able to find all four positions with high accuracy.

For the  $D_{15}$  partial wave we find a rather simple contour, and 2 pole positions can be well located in perfect agreement with SP and RM. However, only the  $D_{15}(1675)^{****}$  lies in our considered range.

For the isospin-3/2  $D$ -wave resonances, PDG reports only one 4-star resonance, the  $D_{33}(1700)^{***}$ . Our analytic results are reproduced well by SP and perfectly by RM. A similar agreement is also found for the resonances  $D_{33}(1940)^*$  and  $D_{35}(11930)^{***}$ . All 3 resonances are located very close to the PDG boxes.

### D. F-waves

Figure 4 displays the  $F$ -wave resonances. The  $F_{15}(1680)^{***}$  is the most important resonance in the 3<sup>rd</sup> resonance region and perfectly described by SP and RM. We also find a weak second  $F_{15}$  state. However, because of its location close to the real axis, this state is also well described by SP and RM. In the vicinity, PDG reports the  $F_{15}(2000)^{**}$  resonance, however, with no pole position given. In the  $F_{17}$  partial wave we can not find a resonance by our analysis, whereas PDG lists a  $F_{17}(1990)^{**}$ . Our result is based on the fact that the inclusion of a bare resonance in this wave does not significantly improve the  $\chi^2$  fit to the data. A similar conclusion was found in Refs. [11, 12].

For the isospin-3/2 resonances, we find three poles as also reported by PDG. The first poles in both partial waves,

$F_{35}(1905)^{***}$  and  $F_{37}(1950)^{***}$ , are well described by SP and RM. However, our positions are significantly above the PDG bounds situated at large imaginary values. This disagreement is not too surprising, because the uncertainty of a pole position rises with the distance from the real axis. We also find a third pole close to the  $F_{35}(2000)^{**}$ , which is however very weak and not well seen in the physical region.

## V. SUMMARY AND CONCLUSION

Within our previously developed Dubna-Mainz-Taipei (DMT) dynamical model we have studied the pole structure of the pion-nucleon  $T$  matrix for all  $S$ ,  $P$ ,  $D$  and  $F$  partial waves in the energy range up to c.m. energy  $W = 2.0$  GeV. We have analytically continued the  $T$  matrix to the unphysical region in the second Riemann sheet and have accurately calculated the pole positions and the residues down to  $\text{Im}W \geq -200$  MeV. These exact values were compared with the results obtained by the speed plot, based on the first derivative of the  $T$  matrix, and a recently developed regularization method using higher derivatives of  $T$ .

Our general conclusions are:

- The number and positions of the DMT poles, obtained by the newly developed analytic continuation method, are in very good agreement with the current PDG results [13].
- All 4-star resonances are nicely reproduced by both the speed-plot technique and the renormalization method. In many cases, however, the latter approach gives significant improvements for the resonance parameters, especially for the pole residues.
- We have confirmed the need for a fourth  $S_{11}$  resonance in addition to the three resonances listed by PDG [13]. The additional  $S_{11}(1878)$  resonance was found to play an important role in pion photoproduction [53], but was not seen in both the  $\pi N \rightarrow \eta N$  reaction and recent data of  $\eta$  photoproduction from the proton [62, 63].
- We have shown that the regularization method is a reliable method to extract the pole parameters from single-channel data. In the absence of a full experimental knowledge about all the channels, this method can be sequentially applied in order to track down the poles relevant for the experimentally known channels of a multichannel amplitude.

## Acknowledgment

S.S.K. wishes to acknowledge the financial support from the National Science Council of ROC for his visits to the Physics Department of National Taiwan University. The work of S.N.Y. is supported in part by the NSC/ROC under grant No. NSC095-2112-M022-025. We are also grateful for the support by the Deutsche Forschungsgemeinschaft through SFB 443, the joint project NSC/DFG 446 TAI113/10/0-3, and the joint Russian-German Heisenberg-Landau program.

---

[1] H.L. Anderson, E. Fermi, E.A. Long, R. Martin, and D.E. Nagle, Phys. Rev. **85**, 934 (1952).  
 [2] E. Fermi, H.L. Anderson, A. Lundby, D.E. Nagle, and G.B. Yodh, Phys. Rev. **85**, 935 (1952).  
 [3] H.L. Anderson, E. Fermi, E.A. Long, and D.E. Nagle, Phys. Rev. **85**, 936 (1952).

- [4] A. Donnachie, Springer Tracts Mod. Phys. **61**, 25 (1972).
- [5] A. Donnachie, Reports on Progress in Physics **36**, 695 (1973).
- [6] G. Höhler, F. Kaiser, R. Koch, and E. Pietarinen, *Handbook of Pion-Nucleon Scattering*, Physics Data 12-1, FIZ Karlsruhe (1979).
- [7] R. Koch and E. Pietarinen, Nucl. Phys. **A336**, 331 (1980).
- [8] R.E. Cutkosky *et al.*, Phys. Rev. D **20**, 2804 (1979).
- [9] R.E. Cutkosky *et al.*, Phys. Rev. D **20**, 2839 (1979).
- [10] R.A. Arndt, J.M. Ford, and L.D. Roper, Phys. Rev. D **32**, 1085 (1985).
- [11] R.A. Arndt, W.J. Briscoe, I.I. Strakovsky, R.L. Workman, and M.M. Pavan, Phys. Rev. C **69**, 035213 (2004).
- [12] R.A. Arndt, W.J. Briscoe, W. J., I.I. Strakovsky, I. I., and R. L. Workman, Phys. Rev. C **74**, 045205 (2006).
- [13] C. Amsler, *et al.* (Particle Data Group), Phys. Lett. B **667**, 1 (2008).
- [14] W. N. Cottingham, D. A. Greenwood, “An Introduction to Nuclear Physics”, Cambridge University Press, Cambridge 1986 and 2001.
- [15] R.H. Dalitz and R.G. Moorhouse, Proc. R. Soc. London A **318**, 279 (1970).
- [16] D. Djukanovic, J. Gegelia and S. Scherer, Phys. Rev. D **76**, 037501 (2007).
- [17] J. Gegelia and S. Scherer, Eur. Phys. Jour. A **44**, 425 (2010).
- [18] G. Höhler, In NSTAR2001, Proceedings of the Workshop on The Physics of Excited Nucleons, ed. D. Drechsel and L. Tiator, World Scientific 2001, 185.
- [19] G.F. Chew, Berkeley UCRL-16983 (1966).
- [20] G. Höhler, D.E. Groom *et al.*, Particle Data Group, Eur. Phys. Jour. **C 15**, 1 (2000).
- [21] G. Höhler and A. Schulte, PiN Newslett. **7**, 94 (1992).
- [22] S. Ceci, J. Stahov, A. Švarc, S. Watson, and B. Zauner, Phys. Rev. **D 77**, 116007 (2008).
- [23] J. von Neumann, E. P. Wigner, Z. Physik **30**, 467 (1929).
- [24] A. Matsuyama, T. Sato, and T.-S. H. Lee, Phys. Rept. **439**, 193 (2007).
- [25] B. Julia-Diaz, T.-S. H. Lee, A. Matsuyama, and T. Sato, Phys. Rev. C **76**, 065201 (2007).
- [26] V. Shklyar, H. Lenske, U. Mosel, and G. Penner, Phys. Rev. C **71**, 055206 (2005).
- [27] M. Döring, C. Hanhart, F. Huang, S. Krewald, and U.-G. Meißner, Nucl. Phys. **A829**, 170 (2009).
- [28] T. Inoue, E. Oset and M.J. Vicente Vacas, Phys. Rev. C **65**, 035204 (2002).
- [29] E.E. Kolomeitsev, M.F.M. Lutz, Phys. Lett. B **585**, 243 (2004).
- [30] G. Y. Chen, S. S. Kamalov, S. N. Yang, Shin Nan, D. Drechsel, and L. Tiator, Phys. Rev. C **76**, 035206 (2007).
- [31] C. Alexandrou, Proc. of NSTAR2009, Beijing, China, 2009, arXiv:0906.4137 [hep-lat].
- [32] A. Walker-Loud *et al.*, Phys. Rev. D **79**, 054502 (2009).
- [33] J. Bulava *et al.*, arXiv:1004.5072 [hep-lat].
- [34] V. Pascalutsa, M. Vanderhaeghen, and S.N. Yang, Phys. Rept. **437**, 125 (2007).
- [35] M. Lüscher, Math. Phys. **105** (1986) 153, Nucl. Phys. B **354** (1991) 531 and Nucl. Phys. B **364** (1991) 237.
- [36] S. Aoki *et al.*, Phys. Rev. D **76**, 094596 (2007).
- [37] V. Bernard, M. Lage, U. G. Meissner and A. Rusetsky, JHEP **0808**, 024 (2008) [arXiv:0806.4495 [hep-lat]].
- [38] S.S. Kamalov, G.Y. Chen, S.N. Yang, D. Drechsel, and L. Tiator, Phys. Lett. B **522**, 27 (2001).
- [39] L. Eisenbud, Ph.D. dissertation, Princeton University 1948, (unpublished).
- [40] F.T. Smith, Phys. Rev. **118**, 349 (1960).
- [41] E.P. Wigner, Phys. Rev. **98**, 145 (1955).
- [42] H.M. Nussenzweig, Phys. Rev. D **6**, 1534 (1972).
- [43] N. Suzuki, T. Sato, and T.-S.H. Lee, Phys. Rev. C **79**, 025205 (2009).
- [44] H. Haberzettl and R. Workman, Phys. Rev. C **76**, 058201 (2007).
- [45] E.P. Wigner and J. von Neumann, Z. Phys. **51**, 844 (1929).
- [46] S. Ceci *et al.*, Phys. Lett. **B 659**, 228 (2008).
- [47] R. L. Workman, R. A. Arndt, M.W. Paris, Phys. Rev. C **79**, 038201 (2009).
- [48] A. Rittenberg *et al.*, (Review of particle properties - particle data group), Rev. Mod. Phys. **43**, S97 (1971).
- [49] G. Höhler in *Landolt-Börnstein: Elastic and Charge Exchange Scattering of Elementary Particles* (Springer-Verlag 1983).
- [50] C.C. Lee, S.N. Yang, and T.-S.H. Lee, J. Phys. **G17**, L131(1991).
- [51] C.T. Hung, S.N. Yang, and T.-S.H. Lee, J. Phys. **G20**, 1531 (1994).
- [52] C.T. Hung, S.N. Yang, and T.-S.H. Lee, Phys. Rev. C **64**, 034309 (2001).
- [53] G.Y. Chen, S.S. Kamalov, S.N. Yang, D. Drechsel, and L. Tiator, Nucl. Phys. A **723**, 447 (2003).
- [54] S.S. Kamalov and S.N. Yang, Phys. Rev. Lett. **83**, 4494 (1999).
- [55] S.S. Kamalov, S.N. Yang, D. Drechsel, O. Hanstein, and L. Tiator, Phys. Rev. C **64**, 032201(R) (2001).
- [56] M. Cooper and B. Jennings, Nucl. Phys. A **500**, 553 (1989).
- [57] S. Morioka and I. R. Afnan, Phys. Rev. C **26**, 1148 (1982).
- [58] B.C. Pearce and I.R. Afnan, Phys. Rev. C **34**, 991 (1986).
- [59] L. Tiator, C. Bennhold, and S. S. Kamalov, Nucl. Phys. A **580**, 455 (1994).
- [60] A. I. L’vov, V. A. Petrun’kin, and M. Schumacher, Phys. Rev. C **55**, 359 (1997).
- [61] D. Drechsel, O. Hanstein, S.S. Kamalov, and L. Tiator, Nucl. Phys. A **645**, 145 (1999).
- [62] U. Thoma, Int. J. Mod. Phys. A **20**, 1568 (2005).
- [63] D. Elsner *et al.* (CBELSA), Eur. Phys. J. A **33**, 147 (2007).
- [64] J. Durand, B. Julia-Diaz, T.-S. H. Lee, B. Saghai, and T. Sato, Int. J. Mod. Phys. A **24**, 553 (2009).

[65] J. Durand, B. Julia-Diaz, T.-S. H. Lee, B. Saghai, and T. Sato, Phys. Rev. C **78**, 025204 (2008).



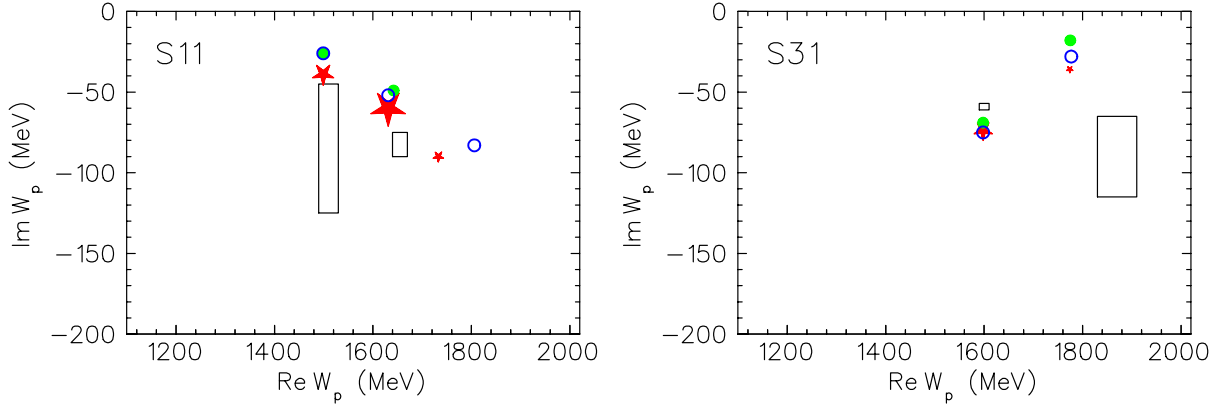


FIG. 1: The pole positions for the  $S$  waves in the complex energy plane. The (red) stars show the results found by analytic continuation, the (green) solid circles and the (blue) open circles are determined by the speed-plot and the regularization methods, respectively. The rectangular regions show the range of the pole positions listed by the Particle Data Group (PDG08) [13]. The size of the (red) stars is proportional to  $|r_p|/\Gamma_p$ , and therefore a measure for the strength of the resonance poles.

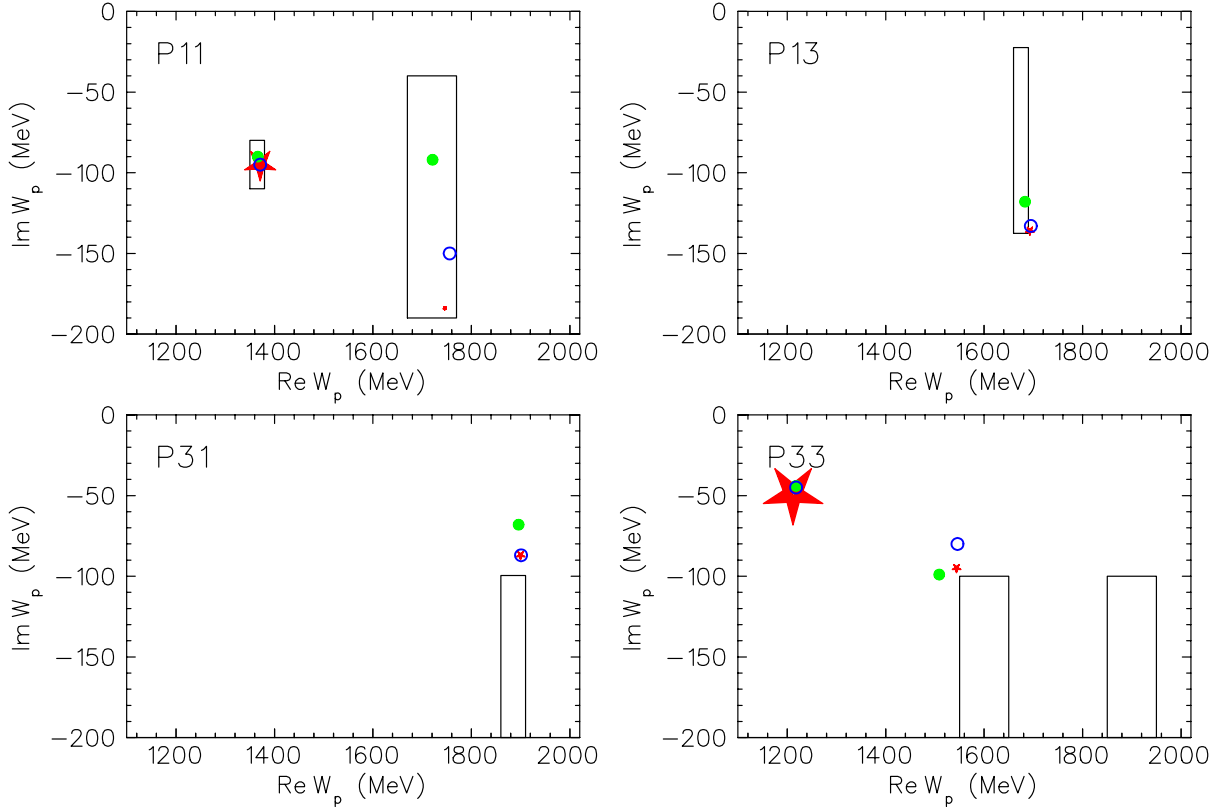


FIG. 2: The pole positions for the  $P$  waves in the complex energy plane. The notation is the same as in Fig. 1.

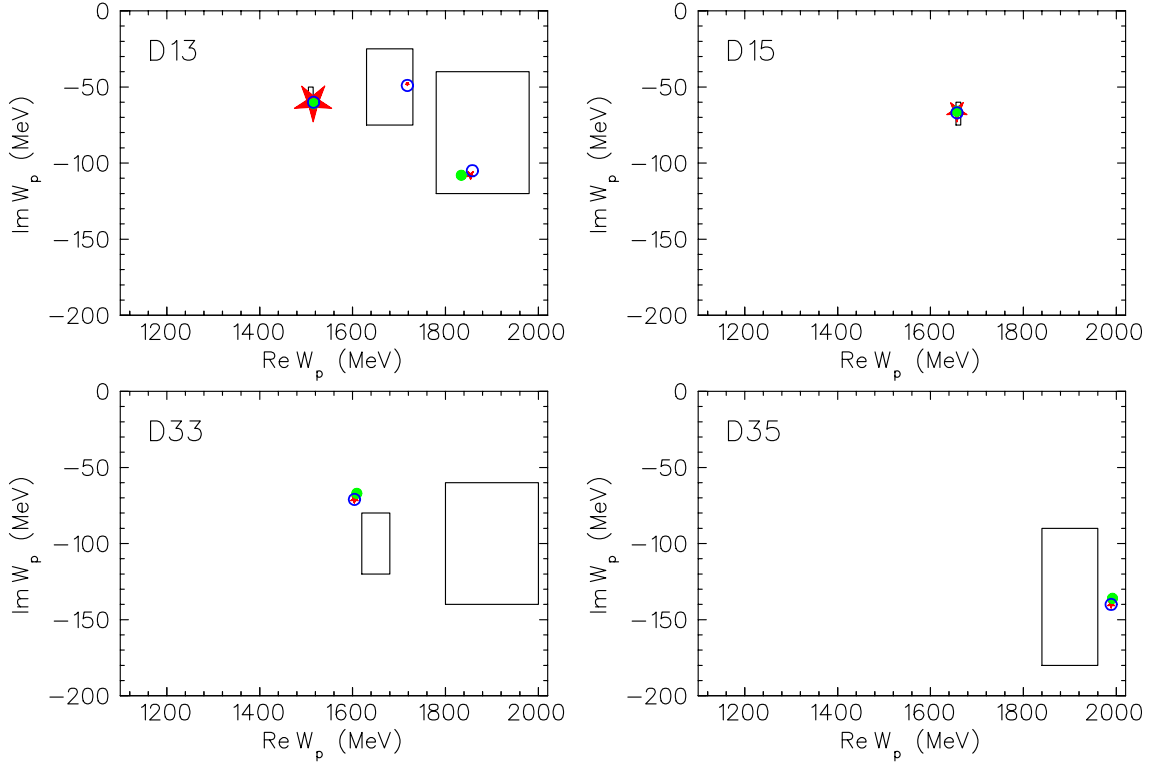


FIG. 3: The pole positions for the  $D$  waves in the complex energy plane. The notation is the same as in Fig. 1.

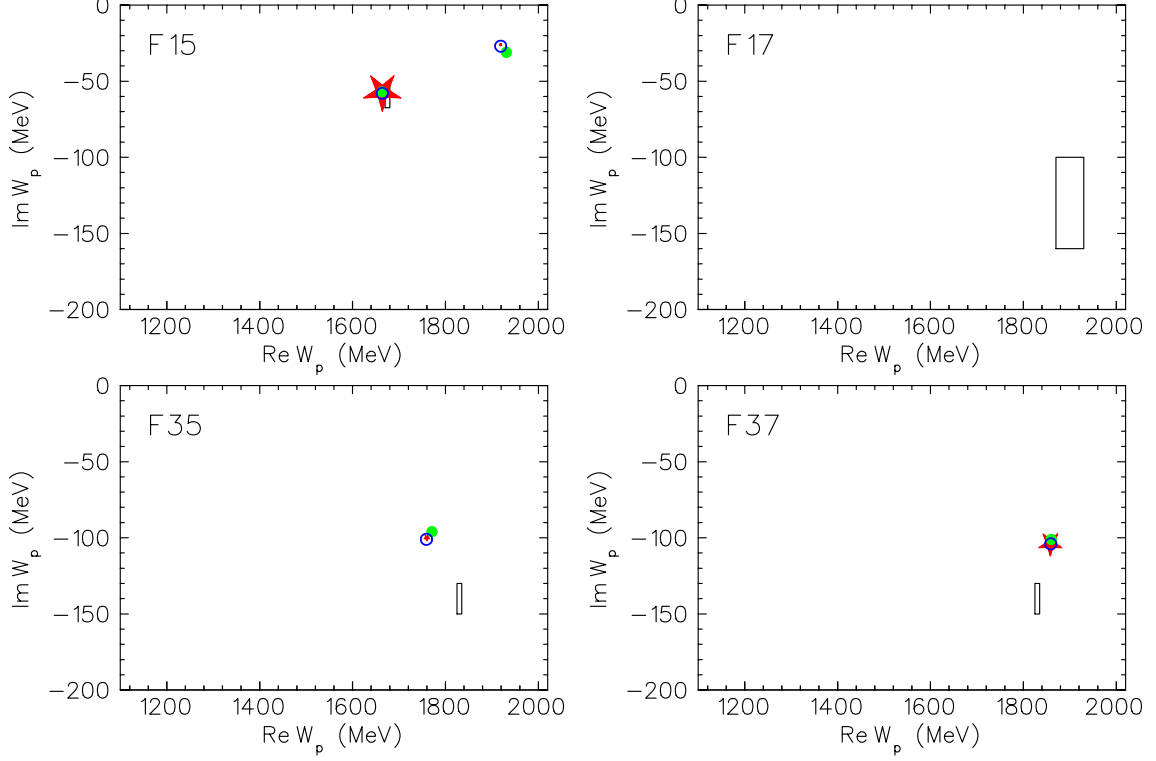


FIG. 4: The pole positions for the  $S$  waves in the complex energy plane. The notation is the same as in Fig. 1.

TABLE I: Pole positions  $W_p = M_p - \frac{1}{2}i\Gamma_p$  and absolute values of the residues  $|r_p|$  at the pole, all in MeV, as well as the phases  $\theta_p$  of the residues for  $S$ -wave resonances. The first lines give the exact pole positions and residues as obtained by analytic continuation of the DMT model, the second and third lines show the values obtained by the speed-plot (SP) and the regularization method (RM(N)) with N being the largest value for stable derivatives. The star classification and the numerical values of the PDG are listed in the last line.

| $N^*$          | $ReW_p$       | $-ImW_p$    | $ r_p $     | $\theta_p(\text{deg})$ |
|----------------|---------------|-------------|-------------|------------------------|
| $S_{11}(1535)$ | 1499          | 39          | 14          | -45                    |
| SP             | 1499          | 26          | 7           | -47                    |
| RM(1)          | 1499          | 26          | 7           | -47                    |
| ****           | $1510 \pm 20$ | $85 \pm 40$ | $96 \pm 63$ | $15 \pm 45$            |
| $S_{11}(1650)$ | 1631          | 60          | 35          | -83                    |
| SP             | 1642          | 49          | 22          | -74                    |
| RM(6)          | 1631          | 52          | 28          | -119                   |
| ****           | $1655 \pm 15$ | $83 \pm 8$  | $55 \pm 15$ | $-75 \pm 25$           |
| $S_{11}(1880)$ | 1733          | 90          | 16          | -29                    |
| SP             | -             | -           | -           | -                      |
| RM(6)          | 1806          | 83          | 10          | -172                   |
| <i>new</i>     |               |             |             |                        |
| $S_{31}(1620)$ | 1598          | 74          | 23          | -98                    |
| SP             | 1598          | 69          | 23          | -99                    |
| RM(6)          | 1598          | 75          | 24          | -100                   |
| ****           | $1600 \pm 10$ | $59 \pm 2$  | $16 \pm 3$  | $-110 \pm 20$          |
| $S_{31}(1900)$ | 1774          | 36          | 3.8         | 179                    |
| SP             | 1775          | 18          | 1.0         | -166                   |
| RM(5)          | 1777          | 28          | 1           | -157                   |
| **             | $1870 \pm 40$ | $90 \pm 25$ | $10 \pm 3$  | $-20 \pm 40$           |

TABLE II: Pole positions residues for  $P$ -wave resonances. For further notation see Tab. I.

| $N^*$          | $ReW_p$        | $-ImW_p$     | $ r_p $     | $\theta_p(\text{deg})$ |
|----------------|----------------|--------------|-------------|------------------------|
| $P_{11}(1440)$ | 1371           | 95           | 50          | -79                    |
| SP             | 1366           | 90           | 48          | -87                    |
| RM(5)          | 1371           | 95           | 50          | -78                    |
| ****           | $1365 \pm 15$  | $95 \pm 15$  | $46 \pm 10$ | $-100 \pm 35$          |
| $P_{11}(1710)$ | 1746           | 184          | 11          | -54                    |
| SP             | 1721           | 92           | 5           | -164                   |
| RM(6)          | 1756           | 150          | 11          | -49                    |
| ***            | $1720 \pm 50$  | $115 \pm 75$ | $10 \pm 4$  | $-175 \pm 35$          |
| $P_{13}(1720)$ | 1693           | 136          | 20          | -43                    |
| SP             | 1683           | 118          | 15          | -64                    |
| RM(4)          | 1695           | 133          | 19          | -34                    |
| ****           | $1675 \pm 15$  | $98 \pm 40$  | $13 \pm 7$  | $-139 \pm 51$          |
| $P_{31}(1910)$ | 1900           | 87           | 13          | -116                   |
| SP             | 1896           | 68           | 7           | -118                   |
| RM(6)          | 1901           | 87           | 10          | -113                   |
| ****           | $1880 \pm 30$  | $100 \pm 20$ | $20 \pm 4$  | $-90 \pm 30$           |
| $P_{33}(1232)$ | 1212           | 49           | 49          | -42                    |
| SP             | 1218           | 44           | 41          | -35                    |
| RM(2)          | 1218           | 45           | 41          | -35                    |
| ****           | $1210 \pm 1$   | $50 \pm 1$   | $53 \pm 2$  | $-47 \pm 1$            |
| $P_{33}(1600)$ | 1544           | 95           | 14          | -111                   |
| SP             | 1509           | 99           | 25          | -197                   |
| RM(5)          | 1546           | 80           | 11          | -116                   |
| ***            | $1600 \pm 100$ | $150 \pm 50$ | $17 \pm 4$  | $-150 \pm 30$          |

TABLE III: Pole positions and residues for  $D$ -wave resonances. For further notation see Tab. I.

| $N^*$          | $ReW_p$        | $-ImW_p$     | $ r_p $     | $\theta_p(\text{deg})$ |
|----------------|----------------|--------------|-------------|------------------------|
| $D_{13}(1520)$ | 1515           | 60           | 40          | -7                     |
| SP             | 1516           | 61           | 40          | -6                     |
| RM(5)          | 1516           | 60           | 40          | -5                     |
| ****           | $1510 \pm 5$   | $55 \pm 5$   | $35 \pm 3$  | $-10 \pm 4$            |
| $D_{13}(1700)$ | 1718           | 48           | 2.8         | -91                    |
| SP             | -              | -            | -           | -                      |
| RM(7)          | 1718           | 49           | 2.9         | -91                    |
| ***            | $1680 \pm 50$  | $50 \pm 25$  | $6 \pm 3$   | $0 \pm 50$             |
| $D_{13}(2080)$ | 1854           | 108          | 16          | -97                    |
| SP             | 1834           | 108          | 14          | -134                   |
| RM(6)          | 1858           | 105          | 9           | -83                    |
| **             | $1950 \pm 170$ | $100 \pm 40$ | $27 \pm 22$ | $\sim 0$               |
| $D_{15}(1675)$ | 1657           | 66           | 24          | -22                    |
| SP             | 1657           | 66           | 24          | -23                    |
| RM(6)          | 1657           | 67           | 25          | -22                    |
| ****           | $1660 \pm 5$   | $68 \pm 6$   | $29 \pm 6$  | $-30 \pm 10$           |
| $D_{33}(1700)$ | 1604           | 71           | 9.4         | -63                    |
| SP             | 1609           | 67           | 9.5         | -52                    |
| RM             | 1604           | 71           | 9.9         | -63                    |
| ****           | $1650 \pm 30$  | $100 \pm 20$ | $13 \pm 3$  | $-20 \pm 25$           |
| $D_{35}(1930)$ | 1989           | 140          | 18          | -78                    |
| SP             | 1992           | 136          | 19          | -75                    |
| RM(5)          | 1989           | 140          | 18          | -78                    |
| ***            | $1900 \pm 50$  | $133 \pm 48$ | $18 \pm 6$  | $-20 \pm 40$           |

TABLE IV: Pole positions and residues for  $F$ -wave resonances. For further notation see Tab. I.

| $N^*$          | $ReW_p$       | $-ImW_p$     | $ r_p $    | $\theta_p(\text{deg})$ |
|----------------|---------------|--------------|------------|------------------------|
| $F_{15}(1680)$ | 1664          | 57           | 38         | -26                    |
| SP             | 1663          | 57           | 38         | -28                    |
| RM(6)          | 1664          | 58           | 39         | -26                    |
| ****           | $1672 \pm 8$  | $61 \pm 6$   | $38 \pm 3$ | $-23 \pm 7$            |
| $F_{15}(2000)$ | 1919          | 26           | 1.0        | 15                     |
| SP             | 1931          | 31           | 1.3        | 89                     |
| RM(4)          | 1919          | 27           | 1.1        | 15                     |
| **             | 1807          | 54.5         | 60         | -67                    |
| $F_{17}(1990)$ | -             | -            | -          | -                      |
| SP             | -             | -            | -          | -                      |
| RM             | -             | -            | -          | -                      |
| **             | $1900 \pm 30$ | $260 \pm 60$ | $9 \pm 3$  | $-60 \pm 30$           |
| $F_{35}(1905)$ | 1760          | 100          | 10         | -66                    |
| SP             | 1771          | 96           | 11         | -47                    |
| RM(5)          | 1759          | 101          | 10         | -66                    |
| ****           | $1830 \pm 5$  | $140 \pm 10$ | $25 \pm 8$ | $-50 \pm 20$           |
| $F_{37}(1950)$ | 1858          | 104          | 43         | -48                    |
| SP             | 1860          | 101          | 44         | -45                    |
| RM(5)          | 1859          | 104          | 44         | -47                    |
| ****           | $1880 \pm 10$ | $140 \pm 10$ | $50 \pm 7$ | $-33 \pm 8$            |